Beyond Classical Limits: Quantum Superposition and Inner Friction in a Quantum Mechanical Engine

Dehua Liu[1,2], Yingying Hong[1], and Jianhui Wang[1*]

[1]*Department of Physics, Nanchang University, Nanchang 330031, China*
[2]*College of Physics and Electronic Science, Hubei Normal University, Huangshi 435002, China*

(Received 28 April 2025; accepted manuscript online 23 June 2025)

We propose a quantum Otto engine operating through a cycle of two isochoric processes, where the working substance interacts with a single-mode radiation field, and two unitary strokes, during which the working substance is decoupled from the field. We investigate the influence of quantum superposition and quantum internal friction on the engine's power output and efficiency, demonstrating that these quantum effects enhance both performance metrics. While these enhancements are accompanied by increased power fluctuations, we show that such fluctuations can be effectively mitigated through careful selection of control parameters. Our results reveal that the proposed quantum Otto engine can achieve performance regimes that are thermally inconceivable in classical systems, including surpassing the Otto efficiency limit and attaining 100% efficiency with nonzero power output.

DOI: 10.1088/0256-307X/42/8/080001 CSTR: 32039.14.0256-307X.42.8.080001

1. Introduction. Quantum heat engines, which harness the principles of quantum mechanics and thermodynamics to perform work, are a promising frontier in energy conversion technology.[1–16] These engines represent an exciting opportunity to explore the interplay between quantum phenomena and thermodynamic processes, unlocking the full potential of quantum resources. With the aid of quantum features such as superposition,[17–20] coherence,[2,21–39] squeezing,[7,40–49] and entanglement,[50–56] atomic-scale energy conversion devices exhibit higher power output, greater efficiency, and lower fluctuations compared to classical counterparts. These features hold the potential to surpass the limitations of classical engines.

Like their classical counterparts, quantum-mechanical engines operate on cyclic models,[17,57,58] such as the Carnot, Brayton, Otto, and Stirling cycles. These engines typically involve energy exchange with the environment, including interactions between the system and an energy bath, along with unitary-driven strokes in which only work is extracted. Unlike thermal engines that rely on thermodynamic principles, quantum engines interact with energy baths (rather than thermal baths) and operate outside the classical confines of the second law of thermodynamics.[59,60] This distinction allows quantum-mechanical engines to exploit the unique properties of quantum mechanics, offering unprecedented performance and control. A key feature of these engines is quantum superposition,[61] which allows particles to exist in multiple states simultaneously, opening up a wealth of possibilities for energy utilization.

Quantum mechanical models of heat engines typically involve particles confined in trapping potentials, such as harmonic[19,58] or box traps.[17,18,57] However, many previous studies have relied on overly simplistic models that neglect the detailed dynamics of the system during the engine cycle. To enhance the performance of these machines in finite time, a more rigorous investigation of energy exchange mechanisms is necessary. This includes analyzing the role of the energy bath, transition rates, and fluctuations,[6,62] as these factors critically impact the performance and reliability of quantum engines.[11,63–69] A thorough understanding of these elements is essential for optimizing the efficiency and functionality of nanoscale engines.

In this Letter, we propose a quantum engine model based on a two-level atomic system coupled to a single-mode radiation field. The engine operates through two isochoric processes, during which the system interacts with the radiation field, and two unitary-driven strokes, where the system evolves in isolation. We analyze the system dynamics for each stroke, focusing on performance and power fluctuations over finite time. Our results show that inner friction, which arises during the unitary-driven strokes in the presence of quantum superposition, can be harnessed as a quantum resource to enhance both power output and efficiency, without compromising the engine's stability. Remarkably, the engine operates beyond the Otto limit in finite time and achieves 100% efficiency, a result that is not constrained by the second law of thermodynamics, as is the case with classical thermal engines.

2. Machine Model. We consider a quantum Otto engine operating with a single qubit. The cycle consists of

*Corresponding author. Email: wangjianhui@ncu.edu.cn
© 2025 Chinese Physical Society and IOP Publishing Ltd. All rights, including for text and data mining, AI training, and similar technologies, are reserved.

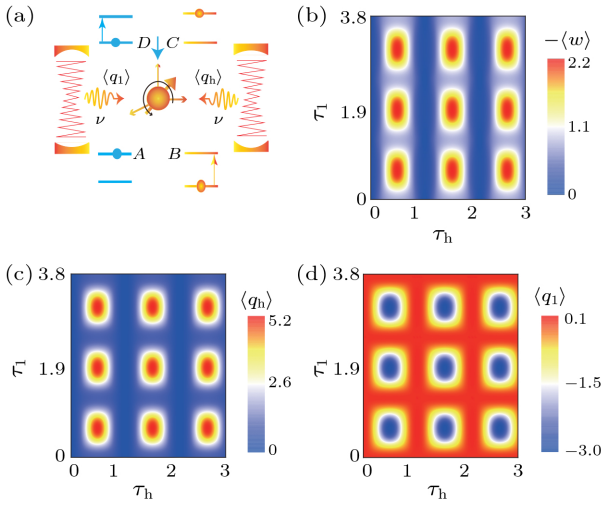

Fig. 1. (a) Schematic of a quantum Otto engine using a two-level atomic system interacting with a single radiation field of frequency ν as the working substance. The cycle consists of two unitary strokes, $A \to B$ and $C \to D$, and two isochoric strokes, $B \to C$ at constant frequency $\omega = \omega_h$ and $D \to A$ at constant frequency $\omega = \omega_l$ ($\omega_l < \omega_h$). The time for completing the high-frequency (low-frequency) isochore is denoted by τ_h (τ_l), while the time for each unitary process is represented by τ_{dr}. In each cycle, the energy injections $\langle q_h\rangle$ and $\langle q_l\rangle$ determine the average work output, $-\langle w\rangle = \langle q_h\rangle + \langle q_l\rangle$. (b), (c), and (d) Contour plots of average work $-\langle w\rangle$, average energy injection $\langle q_h\rangle$, as well as $\langle q_l\rangle$ with respect to τ_h and τ_l when $\tau_{dr} = 0.7$. The parameters are $\omega_l = 1.3\pi$, $\omega_l = 2.2\pi$, $\nu = 1.2\pi$, and $\Omega^r = 1.6\pi$.

two isochoric strokes and two unitary-driven strokes, as illustrated in Fig. 1(a). Thermodynamic transformations are implemented by controlling and deactivating the interaction between the two-level system and a single-mode radiation field.

In the unitary compression stroke ($A \to B$), the system evolves from $t = 0$ to $t = \tau_{dr}$ under a time-dependent frequency $\omega(t)$. The Hamiltonian of the spin-$\frac{1}{2}$ system is given by[4,6]

$$H(t) = \frac{\omega(t)}{2}\Big[\cos\Big(\frac{\pi t}{2\tau_{dr}}\Big)\sigma_x + \sin\Big(\frac{\pi t}{2\tau_{dr}}\Big)\sigma_z\Big],$$

where $\omega(t) = \omega_h(1-t/\tau_{dr})+\omega_l(t/\tau_{dr})$. Here, ω_h and ω_l represent the frequencies associated with the high-frequency and low-frequency isochoric processes, respectively, and σ_x and σ_z represent standard Pauli matrices. During adiabatic process, the linear frequency modulation can be practically realized by controlling external fields, such as microwave or optical fields, with precise timing. This can be achieved using a variable-frequency microwave generator or an optical frequency synthesizer, which allow for the time-dependent modulation of the frequency, as required in the quantum engines.[70] Quantum adiabatic dynamics require slow variations in the Hamiltonian to ensure the system remains in its instantaneous eigenstate. However, for finite-time evolution, deviations from adiabaticity induce quantum inner friction.[4,7,27,71–73] This friction arises from non-commutativity of the Hamiltonian at different times, causing transitions between energy eigenstates. The transition probability, or adiabaticity parameter, is given by

$$\xi \equiv |\langle -(\tau_{dr})|U|+(0)\rangle|^2 = |\langle +(\tau_{dr})|U|-(0)\rangle|^2,$$

where ($\hbar \equiv 1$) the time evolution operator is

$$U = \mathcal{T}_> \exp\Big\{-\mathrm{i}\int_0^{\tau_{dr}} \mathrm{d}t H(t)\Big\},$$

with $\mathcal{T}_>$ denoting time ordering.[4]

Next, in the high-frequency isochoric stroke ($B \to C$), the system couples to a single-mode radiation field of frequency ν for a duration τ_h. The Hamiltonian remains constant, $H = H(\tau_{dr}) = \frac{1}{2}\omega_h\sigma_z$. The system evolves according to the Schrödinger equation,

$$\mathrm{i}\frac{\mathrm{d}|\psi\rangle}{\mathrm{d}t} = (H + H_1)|\psi\rangle, \tag{1}$$

where H and H_1 are the unperturbed and interaction Hamiltonians, respectively. The state at time t is $|\psi(t)\rangle = c_-(t)|-\rangle + c_+(t)|+\rangle$, where $|c_-(t)|^2$ and $|c_+(t)|^2$ are the occupation probabilities of the ground and excited states, satisfying $|c_-(t)|^2 + |c_+(t)|^2 = 1$. Assuming a linearly polarized external field along the x-axis,[74] the interaction Hamiltonian is $H_1 = -ex\mathcal{E}(t) = -(\wp_{-+}|-\rangle\langle+|+\wp_{+-}|+\rangle\langle-|)\mathcal{E}(t)$, where $\wp_{-+} = \wp^*_{+-} = e\langle-|x|+\rangle$ is the matrix element of the electric dipole moment, and $\mathcal{E}(t)$ represents the field interacting with the atom. From Eq. (1), the probability amplitudes $c_+(t)$ and $c_-(t)$ for $\tau_{dr} \le t \le \tau_h + \tau_{dr}$ evolve as

$$\begin{aligned} c_\pm(t) = \Big[c_\pm(0)\Big(\cos\frac{\Omega_h t}{2} \pm \mathrm{i}\frac{\Delta_h}{\Omega_h}\sin\frac{\Omega_h t}{2}\Big) \\ + \mathrm{i}\frac{\Omega^r}{\Omega_h}c_\mp(0)\sin\frac{\Omega_h t}{2}\Big]\mathrm{e}^{\mp\mathrm{i}\Delta_h t/2}, \end{aligned} \tag{2}$$

where $\Delta_h = \omega_h - \nu$ is the detuning, Ω^r is the Rabi frequency, and $\Omega_h = \sqrt{(\Omega^r)^2 + \Delta_h^2}$ is the effective Rabi frequency. A detailed derivation of Eq. (2) is provided in the Supplementary Material (SM).

The unitary expansion stroke reverses the compression protocol over the same duration ($C \to D$), from $t = \tau_{dr} + \tau_h$ to $t = 2\tau_{dr} + \tau_h$, with the Hamiltonian given by $H(t) = H(2\tau_{dr} + \tau_h - t)$. The adiabaticity parameter ξ remains unchanged from the compression stroke.

During the low-frequency isochoric stroke ($D \to A$), the system interacts with the radiation field for a duration τ_l under a constant Hamiltonian, $H = H(0) = \frac{1}{2}\omega_l\sigma_x$, with $\omega_l < \omega_h$. In the time interval $\tau_{cyc} - \tau_l \le t \le \tau_{cyc}$, where the cycle period is given by $\tau_{cyc} = \tau_h + \tau_l + 2\tau_{dr}$, the evolution of the probability amplitudes $c_\pm(t)$ continues to follow Eq. (2). However, in this regime, Δ_h and Ω_h are replaced by Δ_l and Ω_l, respectively. The detuning and effective Rabi frequency are now defined as $\Delta_l = \omega_l - \nu$ and $\Omega_l = \sqrt{(\Omega^r)^2 + \Delta_l^2}$.

For the cyclic engine, all machine variables exhibit periodic behavior,[75,76] meaning the system returns to

its initial state after completing a full cycle.* From this cyclic evolution, we derive expressions for the average work $-\langle w\rangle$, the average energy input $\langle q_{\rm h}\rangle$ during the high-frequency isochore, and the work fluctuations $\delta w_{\rm tot}^2 = \langle w_{\rm tot}^2\rangle - \langle w_{\rm tot}\rangle^2$ as follows:

$$\begin{aligned} -\langle w\rangle &= (w_{\rm h}-w_{\rm l})(p_-^0 - p_-^{\tau_{\rm dr}+\tau_{\rm h}}) \\ &\quad + \xi[w_{\rm h}(1-2p_-^0) + w_{\rm l}(1-2p_-^{\tau_{\rm dr}+\tau_{\rm h}})], \qquad (3)\\ \langle q_{\rm h}\rangle &= w_{\rm h}[\xi + (1-2\xi)p_-^0 - p_-^{\tau_{\rm dr}+\tau_{\rm h}}], \qquad (4)\\ \delta w^2 &= (w_{\rm l}^2 + w_{\rm h}^2)(1-\xi)\xi + [w_{\rm l} + w_{\rm h}(2\xi-1)]^2 p_-^0 \\ &\quad - [w_{\rm h} + w_{\rm l}(2\xi-1)]^2 p_-^{\tau_{\rm dr}+\tau_{\rm h}}(p_-^{\tau_{\rm dr}+\tau_{\rm h}} - 1) \\ &\quad - [w_{\rm l} + w_{\rm h}(2\xi-1)]^2 (p_-^0)^2, \qquad (5)\end{aligned}$$

where $p_-^t = |c_-(t)|^2$ and $p_+^t = |c_+(t)|^2$ denote the occupation probabilities of the ground and excited states at time t. A detailed derivation of Eqs. (3)–(5) is provided in the SM. Using Eqs. (3) and (4), the average energy injection $\langle q_{\rm l}\rangle$ during the low-frequency isochore is given by $\langle q_{\rm l}\rangle = -\langle q_{\rm h}\rangle - \langle w\rangle$.

In Eq. (3), the term $\langle w\rangle_{\rm trl} := (\omega_{\rm h}-\omega_{\rm l})(p_-^0 - p_-^{\tau_{\rm dr}+\tau_{\rm h}})$ represents the average work performed by the system in the transitionless limit, where no transitions between instantaneous energy eigenstates occur. The term $\langle w\rangle_{\rm fri} := \xi[\omega_{\rm h}(1-2p_-^0)+\omega_{\rm l}(1-2p_-^{\tau_{\rm dr}+\tau_{\rm h}})]$ accounts for the additional work required to overcome quantum inner friction,[73] which induces diabatic transitions between energy eigenstates. For the quantum heat engine cycle, p_-^0 and $p_-^{\tau_{\rm dr}+\tau_{\rm h}}$ are consistently greater than 0.5, ensuring that the frictional work remains negative, which implies that friction hinders the system's work output. In contrast, for the quantum mechanical engine, the interaction between the system and the single-mode cavity induces population inversion, thereby allowing the frictional work to potentially become positive. From Eq. (3), the larger the adiabatic parameter ξ, the greater the output work.

Figures 1(b)–1(d) present contour plots of the average work output ($-\langle w\rangle$) and the average energy injected into the system during the two isochores, $\langle q_{\rm l}\rangle$ and $\langle q_{\rm h}\rangle$, as functions of $\tau_{\rm h}$ and $\tau_{\rm l}$. Due to Rabi oscillations in the two-level system under the influence of a single-mode radiation field, the average work output and energy injections exhibit periodic dependence on $\tau_{\rm l}$ and $\tau_{\rm h}$, respectively.

The quantum mechanical engine operates similarly to an external combustion engine, converting energy extracted from an external field into mechanical work through an Otto-like cycle. It functions in two distinct modes. In the conventional thermal engine mode, characterized by $-\langle w\rangle > 0$, $\langle q_{\rm h}\rangle > 0$, and $\langle q_{\rm l}\rangle < 0$, the system absorbs energy from the high-frequency isochore, converts part of it into work, and dissipates the remaining energy during the low-frequency isochore. For the quantum mechanical engine, in the absence of a well-defined concept of heat, the system qualifies as an engine as long as it absorbs energy during one isochoric stroke, performs work, and subsequently releases the residual energy during the other isochoric stroke. This operational criterion aligns with the generalized definition of an engine in the quantum thermodynamic context. The efficiency in this mode is defined as $\eta = -\langle w\rangle/\langle q_{\rm h}\rangle$, where $-\langle w\rangle$ and $\langle q_{\rm h}\rangle$ are defined in Eqs. (3) and (4), respectively. The efficiency is then explicitly given by

$$\eta = 1 - \frac{w_{\rm l}}{w_{\rm h}} + 2\frac{w_{\rm l}}{w_{\rm h}}\frac{\xi(p_-^0 + p_-^{\tau_{\rm dr}+\tau_{\rm h}} - 1)}{p_-^{\tau_{\rm dr}+\tau_{\rm h}} - [\xi(1-2p_-^0) + p_-^0]}. \qquad (6)$$

In contrast, in the second mode, the engine absorbs energy from both the high- and low-frequency isochores, described by $-\langle w\rangle > 0$, $\langle q_{\rm h}\rangle \geq 0$, and $\langle q_{\rm l}\rangle > 0$. In this case, the entire energy input is converted into work, resulting in an efficiency of $\eta = 1$. This mode, unique to quantum mechanical engines, fundamentally differs from conventional thermal engines, which are constrained by the second law of thermodynamics.

The absence of quantum superposition, characterized by $p_-^0 = p_-^{\tau_{\rm dr}} = 1$ and $p_-^{\tau_{\rm dr}+\tau_{\rm h}} = p_-^{\tau_{\rm cyc}-\tau_{\rm l}} = 0$, necessitates that the quantum adiabatic limit ($\xi = 0$) be strictly satisfied for the engine cycle to close.† However, in the presence of quantum superposition, the unitary driving speed may be finite, leading to partial fulfillment of the adiabatic condition, or sufficiently long to fully satisfy it. Therefore, we focus on the engine dynamics when quantum superposition is present, allowing ξ to take either zero or finite values, thereby increasing the engine's operational flexibility.

From Eq. (6), the efficiency reduces to the standard Otto efficiency, $\eta_{\rm Otto} \equiv 1 - \omega_{\rm l}/\omega_{\rm h}$, in two cases: when the quantum adiabatic limit is achieved ($\xi = 0$) and in the absence of state superposition. This observation underscores the crucial role of quantum effects, such as state superposition and quantum inner friction, in modifying the engine's performance. Moreover, since $p_-^0 + p_-^{\tau_{\rm dr}+\tau_{\rm h}} \leq 1$ and $p_-^{\tau_{\rm dr}+\tau_{\rm h}} < p_-^0 + \xi(1-2p_-^0)$, the quantum mechanical engine can achieve efficiencies of $\eta \geq \eta_{\rm Otto}$ over the four

*We focus on the case when the working substance is composed of a two-level system. If external fields are considered as part of the engine system, the energy exchanged between the engine system and its environment is zero. The work done during the system's adiabatic expansion and compression exactly cancels each other out due to energy conservation. Therefore, the engine cannot produce useful work.

†To establish the engine cycle shown in Fig. 1(a), the quantum adiabatic condition must hold without superposition, implying that the ground state probability, p_-^0, must be either 1 or 0. (i) If the system starts in the ground state at point A ($p_-^0 = 1$), the adiabaticity parameter ξ ensures that $0.5 \leq p_-^{\tau_{\rm dr}} \leq 1$ after adiabatic compression. To prevent superposition, the ground state probability at point B must remain 1. During the high-frequency isochoric process, energy absorption requires $p_-^{\tau_{\rm dr}+\tau_{\rm h}} = 0$ at points C and D, ensuring that $p_-^{\tau_{\rm cyc}-\tau_{\rm l}} = p_-^{\tau_{\rm dr}+\tau_{\rm h}}$. The low-frequency isochoric process then restores $p_-^0 = 1$ as energy is released. (ii) If the system begins in the excited state at point A ($p_-^0 = 0$), the ground state probability at point B satisfies $0 \leq p_-^{\tau_{\rm dr}} \leq 0.5$ and must remain 0 to avoid superposition. However, completing the cycle requires energy absorption at point C, which conflicts with the expected energy transfer conditions, as shown in Fig. 1(c). This reinforces the necessity of the quantum adiabatic condition for cycle consistency, under the assumption of $p_-^0 = 1$.

consecutive steps of the cycle (see the SM). Therefore, from Eq. (6), the efficiency increases with a larger adiabaticity parameter ξ. Physically, this enhanced performance arises from population inversion, analogous to that in open quantum systems interfacing with a negative-temperature heat reservoir,[6] thereby enabling operation in regimes inaccessible to classical engines.

Due to the inherent randomness of quantum work, power output fluctuations are significant. Maintaining a consistent and predictable energy flow is essential for the stability of the machine. To evaluate machine stability, we investigate the relative power fluctuation $F_{\rm P} = \sqrt{\delta P^2}/P$, where $\delta P^2 = \langle P^2\rangle - \langle P\rangle^2$ [11] and $P = -\langle w\rangle/\tau_{\rm cyc}$. A lower fluctuation $F_{\rm P}$ indicates that energy transfer processes, such as unitary compression and expansion, are more consistent and less influenced by random fluctuations, enhancing the machine's stability.

Previous studies have shown that internal friction during expansion and compression in quantum thermal engines results in irreversible entropy production, typically leading to negative frictional work.[7] This negative work generally decreases engine performance. However, in quantum mechanical engines, frictional work $\langle w\rangle_{\rm fri}$, like transitionless work $\langle w\rangle_{\rm trl}$, is always positive, as shown in Fig. 2(a). As the driving time $\tau_{\rm dr}$ increases, the frictional work decreases non-monotonically, approaching zero in the quantum-adiabatic limit. This behavior is governed by the adiabaticity parameter ξ, which decreases as the oscillation amplitude diminishes over time. Crucially, the positivity of the frictional work contributes to an increase in the total average work, which combines both transitionless and frictional work, offering a potential avenue for improving engine performance.

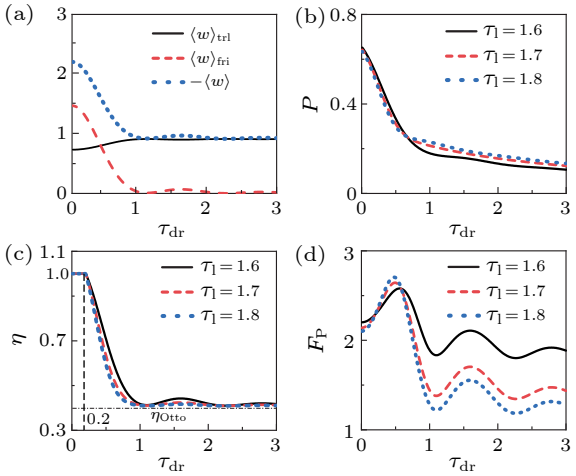

Fig. 2. (a) Average values of total work $-\langle w\rangle$, transitionless work $\langle w\rangle_{\rm trl}$, and frictional work $\langle w\rangle_{\rm fri}$ as functions of the driving time $\tau_{\rm dr}$, evaluated for fixed low-frequency isochore and high-frequency isochore durations $\tau_{\rm l} = 1.6$ and $\tau_{\rm h} = 1.8$. (b) Power output P. (c) Thermodynamic efficiency η as functions of $\tau_{\rm dr}$ for $\tau_{\rm l} = 1.6$, 1.7, and 1.8 at $\tau_{\rm h} = 1.8$. The dot-dashed line indicates the Otto efficiency limit, $\eta_{\rm Otto} = 1 - \omega_{\rm l}/\omega_{\rm h}$. (d) Relative power fluctuation $F_{\rm P}$ as a function of $\tau_{\rm dr}$ for $\tau_{\rm l} = 1.6$, 1.7, and 1.8 at $\tau_{\rm h} = 1.8$. Other parameters are the same as in Fig. 1.

In contrast to thermal engines,[4,7] diabatic transitions due to finite-time operation can significantly enhance both power and efficiency in quantum mechanical engines, as illustrated in Figs. 2(b) and 2(c). While no heat engine can achieve 100% efficiency, a two-level system interacting with a radiation field can produce power equal to its input, thus reaching 100% efficiency. This is shown in Fig. 2(c), where the efficiency $\eta = -\langle w\rangle/(\langle q_{\rm l}\rangle + \langle q_{\rm h}\rangle)$ achieves 100% in the range $0 < \tau_{\rm dr} \leq 0.2$. For $0.2 < \tau_{\rm dr} \leq 3$, efficiency is defined by $\eta = -\langle w\rangle/\langle q_{\rm h}\rangle$. The positive contribution of frictional work at rapid driving speeds leads to a non-monotonic dependence of total average work on $\tau_{\rm dr}$. Consequently, both power and efficiency increase with faster unitary expansion and compression, although the increase is not monotonic. In the quasi-static limit, where the quantum adiabatic condition is satisfied, efficiency approaches the Otto efficiency, as expected from Eq. (6).

As shown in Fig. 2(d), increasing the speed of the quantum engine may lead to either lower or higher relative power fluctuations. Rapid changes in system parameters during fast-driven processes cause the system to transition between different energy eigenstates, resulting in variations in work and large absolute power fluctuations. As the driving speed increases, both power output and absolute power fluctuations rise, causing the relative power fluctuation, which reflects the degree of instability, to either increase or decrease. Thus, with appropriate machine parameters, rapid driving speeds can optimize the quantum engine, with quantum internal friction acting as a lubricant to enhance both efficiency and power, while potentially slightly sacrificing stability or even improving it.

Figure 3 illustrates the average work output, power output, efficiency, and relative power fluctuations as functions of $\tau_{\rm l}$ for varying driving times $\tau_{\rm dr}$, while $\tau_{\rm h}$ is held constant. The average work output, $-\langle w\rangle$, displays periodic behavior as a function of $\tau_{\rm l}$, with a period of $2\pi/\Omega_{\rm l}$, arising from Rabi oscillations at frequency $\Omega_{\rm l}$ [see Fig. 3(a)]. Consequently, the power output decreases periodically with increasing $\tau_{\rm l}$, This behavior can be attributed to the fact that the total cycle time increases with $\tau_{\rm l}$. Since power is defined as work divided by total cycle duration, a longer $\tau_{\rm l}$ leads to reduced power output, as shown in Fig. 3(b). Similarly, the efficiency and relative power fluctuations exhibit periodic trends, sharing the same period $2\pi/\Omega_{\rm l}$ as the work output, as depicted in Figs. 3(c) and 3(d).

A comparison of Figs. 3(a)–3(d) demonstrates that a quantum engine can achieve 100% efficiency, a feat unattainable by classical thermal engines. However, this occurs at the point where efficiency reaches its maximum, coinciding with a peak in relative power fluctuations and a minimum in power output within the cycle. These results, within the framework of tunable system-field interaction times, highlight a trade-off between efficiency, power output, and power fluctuations, analogous to the behavior observed in thermal machines with adjustable system-bath interaction times.[7,68,69,77] Notably, since efficiency, relative power fluctuations, and power output are

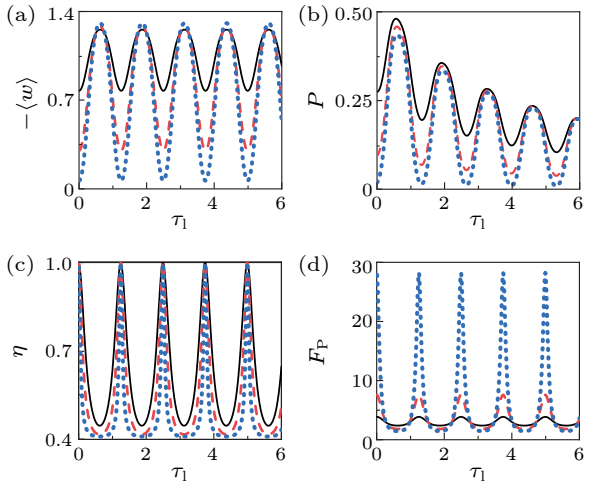

Fig. 3. (a) Average values of total work $-\langle w\rangle$. (b) Power output P. (c) Efficiency η. (d) Relative power fluctuation $F_{\rm P}$ as functions of the time $\tau_{\rm l}$. The results are presented for three different driving durations: $\tau_{\rm dr} = 0.7$ (black solid line), $\tau_{\rm dr} = 0.85$ (red dashed line), and $\tau_{\rm dr} = 1.0$ (green dotted line), with $\tau_{\rm h}$ fixed at 1.8. All other parameters are consistent with those in Fig. 1.

all periodic functions of $\tau_{\rm l}$ with the same period $2\pi/\Omega_{\rm l}$, the engine can be optimized within the regime $0 \leq \tau_{\rm l} \leq \pi/\Omega_{\rm l}$. In this regime, for given values of efficiency and relative power fluctuations, the power output is significantly higher compared to the regime $\pi/\Omega_{\rm l} < \tau_{\rm l} \leq 2\pi/\Omega_{\rm l}$. This underscores the potential to enhance the quantum engine's power output without compromising efficiency or stability, where stability is inversely related to relative power fluctuations.

Optimizing parameters, such as increasing the speed of the unitary-driven stroke or the system-field interaction stroke, can lead to improved performance. Specifically, speeding up the unitary driven strokes results in higher power output and efficiency while simultaneously reducing relative power fluctuations, as also evidenced in Fig. 2. This demonstrates that careful parameter tuning can enhance the overall performance of quantum engines, achieving a balance between power, efficiency, and stability.

During the isochoric strokes, the ion is alternately coupled to a single-mode cavity field or a resonant laser with frequency ν, which is set to be resonant with the $|-\rangle \leftrightarrow |+\rangle$ transition. The state populations p^t_- and p^t_+ are monitored via fluorescence imaging, enabling the extraction of power output, efficiency, and power fluctuations. The experimental setup includes precise control of laser parameters, such as intensity and phase, to ensure accurate Hamiltonian modulation. Additionally, the cavity field is stabilized to maintain consistent coupling strength, while environmental noise is minimized through isolation techniques. Real-time feedback from fluorescence measurements allows for dynamic adjustment of laser parameters to optimize engine performance.

3. Discussions and Conclusions. We have developed a quantum mechanical engine driven by a single-mode radiation field with a constant frequency ν, with periodic adjustments to the strength of the external field. An extension of this engine model involves considering a system where the two isochores occur at different frequencies, $\nu_{\rm h} \neq \nu_{\rm l}$, as discussed in the SM. Using the same methodology as the main model, we conducted numerical calculations to evaluate the average work and energy injections. Our results show that careful selection of the control parameters not only affects the finite-time performance but also enables the system to switch between three operational modes: mechanical engine, refrigerator, and "heater".

We consider the quantized pulse field in the SM, where the semiclassical field is replaced by a quantized single-mode field described by the Jaynes–Cummings model. Despite the quantization of the pulse field, the engine maintains finite power and unit efficiency under short driving times. The thermodynamic behavior remains qualitatively consistent with the semi-classical case, suggesting the feasibility of quantum cavity-based implementations.

We propose a quantum Otto engine that operates through two isochoric processes, where the working substance interacts with a single-mode radiation field, and two unitary strokes, where it evolves in isolation. Quantum superposition and internal friction play a crucial role in enhancing both power output and efficiency. However, they may also introduce power fluctuations, which can be mitigated by appropriately tuning system parameters. Under optimal control, accelerating the engine cycle—either by shortening the unitary strokes or by increasing the system-field interaction rate—can significantly enhance both power and efficiency without increasing the relative power fluctuation. In some cases, this fluctuation, which is directly linked to the machine's stability, may even be reduced. Unlike classical thermal machines that require at least two heat baths, our engine operates with a single energy bath, leveraging quantum superposition and unitary evolution. Remarkably, it can exceed the standard Otto efficiency limit and achieve 100% efficiency while maintaining a finite power output. These findings underscore the potential of quantum thermodynamics in enabling novel energy conversion mechanisms and experimental implementations, particularly in trapped-ion systems and superconducting qubits.

Acknowledgements. We sincerely thank Professor Sumiyoshi Abe for his constructive feedback and rigorous review of an earlier draft of this manuscript. We are also grateful to Professors Wu-Ming Liu, Leilei Yan, and Fei Liu for their insightful discussions. This work was supported by the National Natural Science Foundation of China (Grant No. 12465009). J.W. additionally acknowledges support from the Major Program of Jiangxi Provincial Natural Science Foundation, China (Grant No. 20224ACB201007).

References

[1] Geva E and Kosloff R 1992 *J. Chem. Phys.* **96** 3054
[2] Scully M O, Zubairy M S, Agarwal G S, and Walther H 2003 *Science* **299** 862
[3] Quan H T, Liu Y X, Sun C P, and Nori F 2007 *Phys. Rev. E* **76** 031105

[4] Peterson J P S, Batalhão T B, Herrera M, Souza A M, Sarthour R S, Oliveira I S, and Serra R M 2019 *Phys. Rev. Lett.* **123** 240601
[5] Yang Y Y, Xu S, and He J Z 2020 *Chin. Phys. Lett.* **37** 120502
[6] de Assis R J, de Mendonça T M, Villas-Boas C J, de Souza A M, Sarthour R S, Oliveira I S, and de Almeida N G 2019 *Phys. Rev. Lett.* **122** 240602
[7] Xiao Y, Liu D H, He J Z, Zhuang L, Liu W M, Yan L L, and Wang J H 2023 *Phys. Rev. Res.* **5** 043185
[8] Holubec V and Ryabov A 2018 *Phys. Rev. Lett.* **121** 120601
[9] von Lindenfels D, Gräb O, Schmiegelow C T, Kaushal V, Schulz J, Mitchison M T, Goold J, Schmidt-Kaler F, and Poschinger U G 2019 *Phys. Rev. Lett.* **123** 080602
[10] Koch J, Menon K, Cuestas E, Barbosa S, Lutz E, Fogarty T, Busch T, and Widera A 2023 *Nature* **621** 723
[11] Bouton Q, Nettersheim J, Burgardt S, Adam D, Lutz E, and Widera A 2021 *Nat. Commun.* **12** 2063
[12] Das D, Thomas G, and Jordan A N 2023 *Phys. Rev. A* **108** 012220
[13] Brandner K, Bauer M, Schmid M T, and Seifert U 2015 *New J. Phys.* **17** 065006
[14] Fadler P, Friedenberger A, and Lutz E 2023 *Phys. Rev. Lett.* **130** 240401
[15] Yuan J H, Ruan H L, Liu D H, He J Z, and Wang J H 2023 *Chin. Phys. Lett.* **40** 096301
[16] Wang C, Ren J, and Cao J S 2017 *Phys. Rev. A* **95** 023610
[17] Abe S 2011 *Phys. Rev. E* **83** 041117
[18] Abe S and Okuyama S 2012 *Phys. Rev. E* **85** 011104
[19] Jie O C, Fu H Z, Hong L B, and Chen J C 2013 *Sci. China Phys. Mech. Astron.* **57** 1266
[20] Hardal A Ü C and Müsteçaplıoğlu Ö E 2015 *Sci. Rep.* **5** 12953
[21] Liang Z T, Lv Q X, Zhang S C, Wu W T, Du Y X, Yan H, and Zhu S L 2019 *Chin. Phys. Lett.* **36** 080301
[22] Rahav R, Harbola U, and Mukamel S 2012 *Phys. Rev. A* **86** 043843
[23] Goswami H P and Harbola U 2013 *Phys. Rev. A* **88** 013842
[24] Lostaglio M, Jennings D, and Rudolph T 2015 *Nat. Commun.* **6** 6383
[25] Santos J P, Céleri L C, Landi G T, and Paternostro M 2019 *npj Quantum Inf.* **5** 23
[26] Klatzow J, Becker J N, Ledingham P M, Weinzetl C, Kaczmarek K T, Saunders D J, Nunn J, Walmsley I A, Uzdin R, and Poem E 2019 *Phys. Rev. Lett.* **122** 110601
[27] Baumgratz T, Cramer M, and Plenio M B 2014 *Phys. Rev. Lett.* **113** 140401
[28] Roßnagel J, Abah O, Schmidt-Kaler F, Singer K, and Lutz E 2014 *Phys. Rev. Lett.* **112** 030602
[29] Korzekwa K, Lostaglio M, Oppenheim J, and Jennings D 2016 *New J. Phys.* **18** 023045
[30] Zhang L, Tian T, Huang P, Lin S C, and Du J F 2020 *Chin. Phys. Lett.* **37** 014501
[31] Brandner K, Bauer M, and Seifert U 2017 *Phys. Rev. Lett.* **119** 170602
[32] Streltsov A, Adesso G, and Plenio M B 2017 *Rev. Mod. Phys.* **89** 041003
[33] Kilgour M and Segal D 2017 *Phys. Rev. E* **98** 012117
[34] Dorfman K E, Xu D Z, and Cao J S 2018 *Phys. Rev. E* **97** 042120
[35] Francica G, Goold J, and Plastina F 2019 *Phys. Rev. E* **99** 042105
[36] Camati P A, Santos J F G, and Serra R M 2019 *Phys. Rev. A* **99** 062103
[37] Zicari G, Çakmak B, Müsteçaplıoğlu Ö E, and Paternostro M 2023 *New J. Phys.* **25** 013030
[38] Um J, Dorfman K E, and Park H 2022 *Phys. Rev. Res.* **4** L032034
[39] Lu J C, Wang Z, Ren J, Wang C, and Jiang J H 2024 *Phys. Rev. B* **109** 125407
[40] Liu H G, He J Z, and Wang J H 2023 *Chin. Phys. B* **32** 030503
[41] Zhang Y C 2020 *Physica A* **559** 125083
[42] Klaers J, Faelt S, Imamoglu A, and Togan E 2017 *Phys. Rev. X* **7** 031044
[43] Yin Q, Xiang G Y, Li C F, and Guo G C 2018 *Chin. Phys. Lett.* **35** 070302
[44] Huang X L, Wang T, and Yi X X 2012 *Phys. Rev. E* **86** 051105
[45] de Assis R J, Sales J S, da Cunha J A R, and de Almeida N G 2020 *Phys. Rev. E* **102** 052131
[46] Agarwalla B K, Jiang J H, and Segal D 2017 *Phys. Rev. B* **96** 104304
[47] Altintas F, Hardal A Ü C, and Müsteçaplıoğlu Ö E 2014 *Phys. Rev. E* **90** 032102
[48] Werlang T, Guzmán R, Prado F O, and Villas-Bôas C J 2008 *Phys. Rev. A* **78** 033820
[49] Liu H G 2024 *Chin. Phys. B* **33** 100503
[50] Zhang T, Liu W T, Chen P X, and Li C Z 2007 *Phys. Rev. A* **75** 062102
[51] Wu F L, Liu S Y, Yang W L, and Fan H 2019 *Chin. Phys. Lett.* **36** 060301
[52] Wang K K, Xia R Q, Bresque L, and Xue P 2022 *Phys. Rev. Res.* **4** L032042
[53] Bresque L, Camati P A, Rogers S, Murch K, Jordan A N, and Auffèves A 2021 *Phys. Rev. Lett.* **126** 120605
[54] Josefsson M and Leijnse M 2020 *Phys. Rev. B* **101** 081408
[55] Ji Y H, Hu J J, and Hu Y 2012 *Chin. Phys. B* **21** 110304
[56] Oliveira M H, Higgins G, Zhang C, Predojević A, Hennrich M, Bachelard R, and Villas-Boas C J 2023 *Phys. Rev. A* **107** 023706
[57] Bender C M, Brody D C, and Meister B K 2000 *J. Phys. A* **33** 4427
[58] Wang J H, He J Z, and He X 2011 *Phys. Rev. E* **84** 041127
[59] Abe S and Okuyama S 2011 *Phys. Rev. E* **83** 021121
[60] Bender B, Brody D, and Meister B 2002 *Proc. R. Soc. A* **458** 1519
[61] Dirac P A M 1958 *The Principles of Quantum Mechanics* (Oxford: Clarendon Press)
[62] Yang F B, Zhang Z R, Xu L J, Liu Z F, Jin P, Zhuang P F, Lei M, Liu J R, Jiang J H, Ouyang X P, Marchesoni F, and Huang J P 2024 *Rev. Mod. Phys.* **96** 015002
[63] Denzler T and Lutz E 2020 *Phys. Rev. Res.* **2** 032062
[64] Talkner P, Lutz E, and Hänggi P 2017 *Phys. Rev. E* **75** 050102
[65] Wang R, Wang C, Lu J, and Jiang J H 2022 *Adv. Phys. X* **7** 2082317
[66] Segal D 2018 *Phys. Rev. E* **97** 052145
[67] Denzler T and Lutz E 2021 *Phys. Rev. Res.* **3** L032041
[68] Funo K and Ueda M 2015 *Phys. Rev. Lett.* **115** 260601
[69] Denzler T and Lutz E 2021 *New J. Phys.* **23** 075003
[70] Levy A and Kosloff R 2012 *Phys. Rev. Lett.* **108** 070604
[71] Rezek Y and Kosloff R 2017 *Entropy* **19** 136
[72] Jiao G Q, Zhu S B, He J Z, Ma Y L, and Wang J H 2021 *Phys. Rev. E* **103** 032130
[73] Plastina F, Alecce A, Apollaro T J G, Falcone G, Francica G, Galve F, Lo Gullo N, and Zambrini R 2014 *Phys. Rev. Lett.* **113** 260601
[74] Scully M O and Zubairy M S 1997 *Quantum Optics* (Cambridge: Cambridge University Press)
[75] Feldmann T and Kosloff R 2004 *Phys. Rev. E* **70** 046110
[76] Liu J J, Jung K A, and Segal D 2021 *Phys. Rev. Lett.* **127** 200602
[77] Miller H J D, Mohammady M H, Perarnau-Llobet M, and Guarnieri G 2021 *Phys. Rev. Lett.* **126** 210603